

**Effect of Copper Oxide addition on Dielectric and
Magnetic Properties of Zn-Ti Substituted
Sr-M Hexagonal Ferrite**

A THESIS SUBMITTED IN PARTIAL FULFILLMENT OF
THE REQUIREMENTS FOR THE DEGREE OF
BACHELOR OF TECHNOLOGY

By

ABHISEK SAHOO

Roll no: - 111CR0108



**DEPARTMENT OF CERAMIC ENGINEERING
NATIONAL INSTITUTE OF TECHNOLOGY
ROURKELA
2014-2015**

**Effect of Copper Oxide addition on Dielectric and
Magnetic Properties of Zn-Ti Substituted
Sr-M Hexagonal Ferrite**

A THESIS SUBMITTED IN PARTIAL FULFILLMENT OF
THE REQUIREMENTS FOR THE DEGREE OF
BACHELOR OF TECHNOLOGY

By

ABHISEK SAHOO

Roll no: - 111CR0108

UNDER THE GUIDANCE OF
DR. JAPES BERA



**DEPARTMENT OF CERAMIC ENGINEERING
NATIONAL INSTITUTE OF TECHNOLOGY
ROURKELA
2014-2015**



**NATIONAL INSTITUTE OF TECHNOLOGY
ROURKELA**

CERTIFICATE

This is to certify that the thesis entitled, “**Effect of Copper Oxide addition on Dielectric and Magnetic Properties of Zn-Ti Substituted Sr-M Hexagonal Ferrite**”, submitted by **Abhisek Sahoo** in partial fulfilment of the requirements of the award of *Bachelor of Technology Degree in Ceramic Engineering at National Institute Of Technology, Rourkela* is an authentic work carried out by him under my supervision and guidance.

To the best of my knowledge, the matter embodied in the thesis has not been submitted to any other university/institute for the award of any Degree or Diploma.

Date: 29.06.2015

Dr. Japes Bera
(Associate Professor)
Dept. of Ceramic Engineering
National Institute of Technology
Rourkela-769008

Acknowledgement

I wish to express my deep sense of respect and regard for Prof. Japes Bera, Department of Ceramic Engineering, and N.I.T Rourkela for introducing the research topic and for his inspiring guidance, constructive criticism and valuable suggestions throughout this research work. I would also like to thank him for his constant support and words of encouragement without which it would not have been possible for me to complete this research work.

I am also grateful to all the faculty members of the Dept. of Ceramic Engineering, whose immense knowledge in the field of ceramics has enlightened me in various areas of my research work.

I am also grateful to Mr. Vikash Kumar Patel, Mr. Ganesh Kumar Sahoo, Miss Geetanjali Parida and all the other research scholars in the Dept. of Ceramic Engineering for their unparalleled help and support.

Finally, I deeply thank my parents for all their support and faith in me.

Abhisek Sahoo

Date: 29.06.2015

ABHISEK SAHOO
Roll No: - 111CR0108
B.Tech, Dept. of Ceramic Engineering
N.I.T Rourkela

ABSTRACT

Sr-M-Hexagonal ferrite is an important ferrite for industrial application. Magnetic properties of the ferrite are usually improved by the substitution of Ti and Zn for iron in the hexagonal ferrite structure. In the present investigation, Zn and Ti have been substituted in the Sr-M-hexagonal ferrite as per the formula $\text{SrZn}_{1.3}\text{Ti}_{1.3}\text{Fe}_{9.4}\text{O}_{19}$. Effect of CuO sintering additives was investigated on the ferrite as per the composition $\text{SrZn}_{1.3}\text{Ti}_{1.3}\text{Cu}_x\text{Fe}_{9.4-x}\text{O}_{19-z}$ with $x=0.5$ and 1.0 . The ferrite has been synthesized through nitrate-citrate sol-gel combustion route. The decomposition behaviour of the gel has been investigated using DSC-TG analysis. The as burnt powder was finally calcined at 1200°C . The phase formation behaviour during calcination and after sintering has been investigated using X-ray powder diffraction analysis. Effect of CuO sintering additives on densification behaviour was investigated on the sintered pellet by measuring bulk density and apparent porosity. Similarly, its effect on the dielectric and magnetic properties of the ferrite has been investigated by measuring permittivity on pellet sample and magnetic permeability on torroid sample. The microstructural development of the ferrite was investigated using scanning electron microscope. Finally the changes in properties of the ferrite due to the addition of CuO have been explained and correlated. It has been found that the CuO addition was very effective for the phase formation and improved densification and hence improved magneto-dielectric properties of the ferrite.

Chapter 1

Introduction

Introduction:

In recent years, there has been increasing degree of interest in the hexagonal ferrites. These have become massively important materials commercially and technologically, accounting for the bulk of the total magnetic materials manufactured globally, and they have a multitude of uses and applications. Besides their use as permanent magnets, other common applications are as magnetic recording and data storage materials, and as components in electrical devices, particularly those operating at microwave/GHz frequencies [1].

The group of ferrites having hexagonal crystal structures is called hexagonal ferrite or hexa-ferrite. There are numbers of hexa-ferrite compound in the general composition $\text{BaO-MeO-Fe}_2\text{O}_3$, where Me is a small 2+ ion such as cobalt, nickel or zinc, and Ba can be substituted by Sr. Important types of hexa-ferrites are designated as M, W, Y, Z, X and U types. The chemical formulas of them are:

- M-type: $\text{BaFe}_{12}\text{O}_{19}$ (BaM) or $\text{SrFe}_{12}\text{O}_{19}$ (SrM),
- W-type: $\text{BaMe}_2\text{Fe}_{16}\text{O}_{27}$,
- Y-type: $\text{Ba}_2\text{Me}_2\text{Fe}_{12}\text{O}_{22}$,
- Z-type: $\text{Ba}_3\text{Me}_2\text{Fe}_{24}\text{O}_{41}$,
- X-type: $\text{Ba}_2\text{Me}_2\text{Fe}_{28}\text{O}_{46}$,
- U-type: $\text{Ba}_4\text{Me}_2\text{Fe}_{36}\text{O}_{60}$.

They are all ferrimagnetic materials and their magnetic properties are intrinsically linked to their crystal structure. All have magneto-crystalline anisotropy (MCA) that is the induced magnetisation has a preferred orientation within the crystal structure. On the basis of MCA, they can be divided into two main groups, those with

- (1) Easy axis of magnetisation, the **uniaxial** hexaferrites and
- (2) Easy plane (or cone) of magnetisation, known as **hexaplana** ferrites

M, Z, W, X and U-types ferrites are uniaxial and Y-type is hexaplana ferrites. However, Co_2Z , Co_2W , Co_2X and Co_2U ferrites have planar anisotropy [2].

The compound with greatest technological interest is M-hexagonal ferrites. They are magnetically very hard materials due to their uniaxial and high MCA constants. Their magnetisation is locked rigidly along the preferred *c*-axis of the hexagonal structure. The high MCA is prerequisite for a high coercivity, which results a magnetically hard material suitable for permanent magnets. On the other hand, hexaplana ferrites have a preferred direction of magnetization either in the hexagonal basal plane or in a cone and they are excellent soft magnet due to free rotation of magnetisation in the plane/cone. It has been reported that ferrites with planar MCA exhibit good magnetic performance in the GHz range and have higher resonance frequency compared to spinel ferrites [1]. To make them more useful in high frequency GHz application, M-ferrites are substituted with different cations (for example, Co^{2+} and Ti^{4+} for Fe^{3+}), which changes its MCA from uniaxial to planar type.

For high frequency application, the MW dielectric losses of ferrites must be minimized. The dielectric losses due to the damping of the vibration of electrical dipoles, dominate at higher frequencies, causing a high decrease of permittivity in most materials. For that reason, ferrites must have good electrical insulation and moderate permittivity to allow the full penetration of electrical field. Most hexagonal ferrites are better than cubic spinel ferrite with respect to above two properties and therefore are well suited for high frequency applications.

In addition to the high operating frequency, current generation electronic devices are becoming smaller with less weight and more efficient day by day. For that, the passive components are used in the form of multilayer chip component and are surface mounted

on printed circuit boards. The recent trend is the integration of different passive components onto a single Si-wafer platform enabling more reduction of device volume and weight. For both the technologies, low temperature co-fired ceramics (LTCC) is required for co-sintering with internal metal electrode. One of such component is multilayer ferrite chip inductor (MLFCI) shown in Fig.1.

Construction

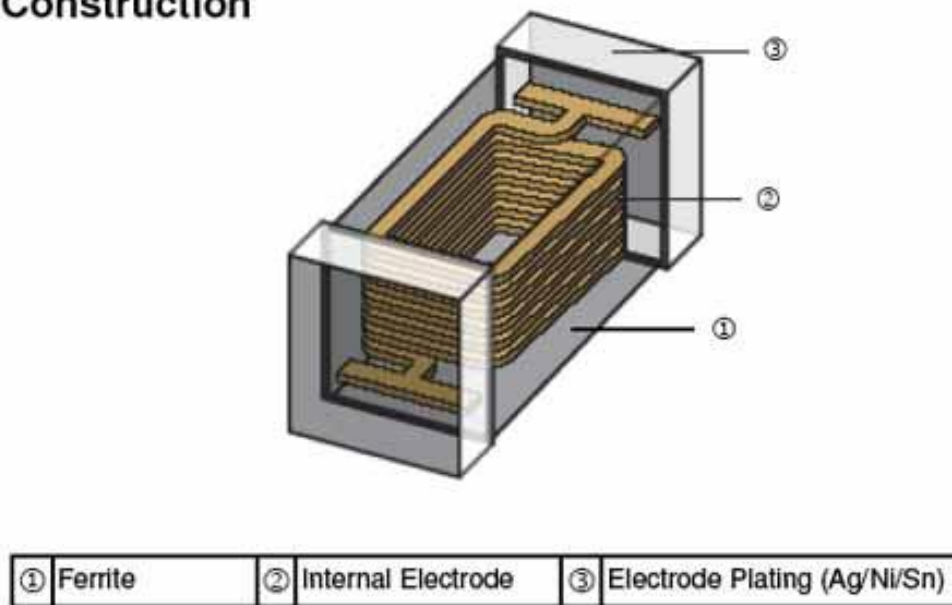


Fig-1- multilayer ferrite chip inductor (MLFCI).

$\text{SrFe}_{12}\text{O}_{19}$ is an important magnetic hexa-ferrite which is used for high frequency application in multilayer chip inductor. Generally $\text{BaFe}_{12}\text{O}_{19}$ is used for such high frequency applications but it has been observed that $\text{SrFe}_{12}\text{O}_{19}$ has better magnetic properties than the prior at high frequency range.

Ferrite	Formula	M_s ($\text{A m}^2 \text{ kg}^{-1}$)	H_a (kA m^{-1})	K_1 (erg/cm^3)	T_c ($^\circ\text{C}$)
BaM	$\text{BaFe}_{12}\text{O}_{19}$	72	1353	3.3×10^6	450
SrM	$\text{SrFe}_{12}\text{O}_{19}$	92-74	1592	3.5×10^6	460

For the fabrication of MLFCI, ferrite is co-sintered with an internal metal. The structure and manufacturing process of MLFCI is shown in Fig.3. Silver (Ag) is usually most suitable internal electrode as it has;

- High conductivity
- Lower cost
- Lower electrical losses.

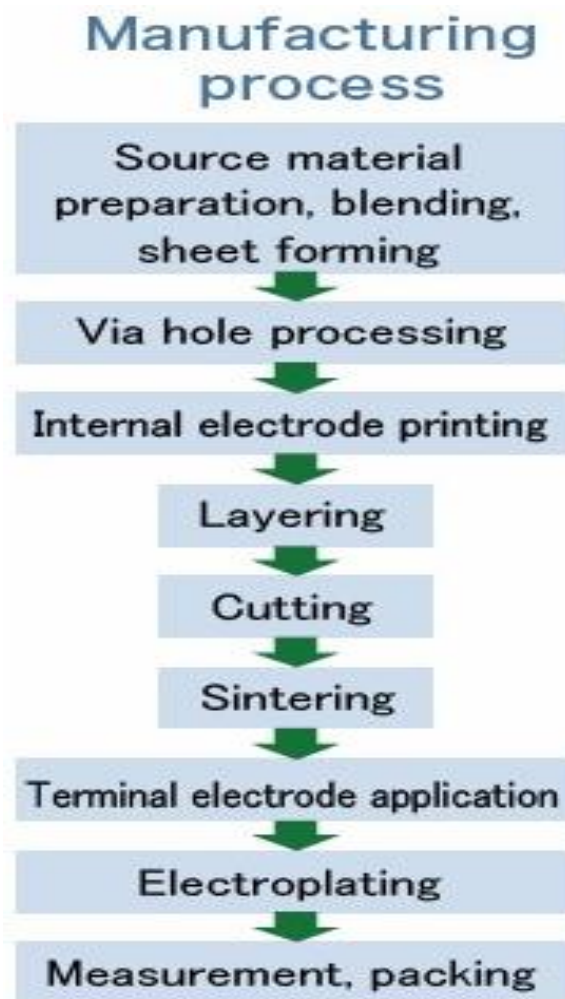


Fig.2- manufacturing process of multilayer chip inductor.

As silver melts at 961°C , the ferrite composition must be co-sintered at a temperature sufficiently lower than that, preferably at 900°C , to prevent possible diffusion of Ag into the ferrite. Otherwise the diffusion of Ag metal may decrease the permeability of the

ferrite. For low temperature sintering of the ferrites, usually sintering additives like glass, Bi_2O_3 , are used. However, the sintering additive decreases the permeability of ferrite, and the quantity of additive should be as low as possible. Additionally, sinter-active fine ferrite powders are used for chip fabrication. Another solution could be a suitable modification of the ferrite composition enabling its low temperature sintering. As mentioned above, a recent patent [5] discloses such a modified composition of BaM ferrite which is capable of being sintered at 920°C without the use of any sintering additive.

Substituted Z and Y-type hexaplana ferrites are also used for GHz applications. However, they are not so compatible with the LTCC multilayer technology. Their synthesis requires high temperatures which contradicts the required low-temperature sintering behaviour of MLFCI [7].

With this background, it may be concluded that SrM ferrite will be a good candidate for high frequency chip application with respect to the enhancement of SRF. As stated above, SrM ferrite has higher saturation magnetization and magnetic anisotropy field H_a than BaM ferrite and expected to show better high frequency properties compared to BaM ferrite.

Chapter 2

Literature

review

In this section an effort has been made to provide a detailed review of the research work undertaken by various researchers on the synthesis of $\text{SrFe}_{12}\text{O}_{19}$ and the effect of doping of different amount of divalent cations on the magnetic and electric property as well as the effect of various sintering additives on the sintering temperature.

Numerous examination works have been completed to enhance the electro-magnetic properties of $\text{SrFe}_{12}\text{O}_{19}$. One of these endeavours is by the substitution of different divalent cations like Co, Ti, Zn, and La (trivalent) in $\text{SrFe}_{12}\text{O}_{19}$.

The Sr-M ferrites have been synthesized through different routes like; conventional solid oxide reaction [12], co-precipitation [13], sol-gel [14], hydrothermal [15], glass crystallization [16], combustion method [17], etc. The phase formation of these hexaferrites is an extremely complicated process and their formation mechanisms are not yet fully understood [2]. SrM has been synthesized through conventional solid oxide reaction by calcining oxide raw materials at 1000o C for 12 hrs. [12]. However, the phase can be synthesized at a temperature as low as 700o C by sol-gel processing [14]. So the sol-gel processing could be an effective route for the synthesis of fine-grained sinter-active ferrite powders.

Magnetic properties of the ferrite depend on many parameters like density, grain size, chemical composition and grain alignment. In general, higher is the density higher will be saturation magnetization (M_s) and lower the grain size higher will be coercive field (H_c). The cation substitution is one of the most important methods for improving magnetic properties of ferrites. M_s of the ferrite can be increased by the substitution of non-magnetic Zn^{2+} for Fe^{3+} , where Zn^{2+} prefers tetrahedral positions of the crystal structure.

The substitution reduces the negative contribution of tetrahedral-octahedral anti-ferromagnetic coupling. Other 2-valence cations like Cu, Ni, Co, Mg and Mn have also been substituted for Fe^{3+} . The charge compensation for these substitutions is done either by

substituting Ba with 3-valence cation or by substituting Fe with 4-valence cation. Different 3-valence cations like V, Ga, Al, In or Sc and 4-valence cations like Ti, Sn, Zr, Hf, Ce or Ru have been substituted in the ferrite.

The most common substitution in M-ferrite is $\text{BaCo}_x\text{Ti}_x\text{Fe}_{12-2x}\text{O}_{19}$ and the substitution is very important for tailoring anisotropy and microwave properties of M-ferrite [2]. With the increase in x , grain size, M_s and H_c decreases. Ti plays major role in decreasing grain size and Co plays role in the change of magnetic properties. The axial anisotropy of the ferrite decreases with the substitution and converted into in-plane anisotropy. Hence, a very soft ferrite can be achieved with the substitution while keeping M_s Value reasonably stable. Other major advantage of $\text{Co}^{+2}/\text{Ti}^{+4}$ substitutions is increased resistivity of the substituted ferrite. Similar behaviour is found in other substitutions like; CoZr-M , CoSn-M , NiZnTi-M .

It has been found that a stoichiometric mixture of ferrite powders never sinter fully, whereas Fe deficient material can be fully densified. This is attributed to increased diffusion rates in the non-stoichiometric mixes due to induced lattice defects. For co-sintering with Ag internal electrode in a MLFCI, the sintering temperature of ferrite must be reduced to 900o C or less. Two most effective approaches to reduce the sintering temperature are (1) Use of additives like glass, B_2O_3 , SiO_2 , for liquid phase sintering and (2) Partial substitution of metal cations by Cu or addition of CuO. There are only few reports on reduction of sintering temperature of Sr-M ferrite by CuO addition [18, 19]. The major mechanism proposed [12] for enhanced sintering was the formation of Cu-rich eutectic phase which melts below 1000o C and enabled the reactive liquid-phase sintering of CuO added SrM ferrite. They also proposed that Cu^{2+} was not substituted in hexagonal structure, rather spinel type Cu-ferrite and Cu-rich eutectic phases were formed.

There are very few international patents on this typical issue. The patent on "Ferrite Material for a Permanent Magnet and Method for Production There of"[18], revealed about low

temperature sintered Sr-M ferrite for MLFI application. In any case, one late patent [5] uncovers about the synthesis taking into account the low temperature sintered Ba-M ferrite for chip bead and antenna application in few 500 MHz frequency band.

Muhammad Naeem Ashiq, Raheela Beenish Qureshia, Muhammad Aslam Malana and Muhammad Fahad Ehsanb [19] synthesized Zirconium copper substituted calcium strontium hexagonal ferrites with composition $\text{Ca}_{0.5}\text{Sr}_{0.5}\text{Fe}_{12-2x}\text{Zr}_x\text{Cu}_x\text{O}_{19}$ ($x=0.0, 0.2, 0.4, 0.6, 0.8$) by the chemical co precipitation procedure. The dielectric parameters show relaxation behaviour at higher frequencies. The values of dielectric parameters increase with dopants. In the range of magnetic field studied, the saturation magnetization decreases as the dopant contents increase which may be due to the nonmagnetic character of the substituents. The coercivity of the Zr-Cu doped derivatives of strontium calcium hexaferrites is increased up to $x=0.2$ and then decreased. The values of coercivity are above 600Oe which make them suitable materials for use in industries in longitudinal magnetic recording media.

Ali Ghasemiet. al. [21] prepared Sn and Zn substituted Strontium hexa-ferrite by a sol-gel process on thermally oxidized silicon wafer (Si/SiO₂). The SEM analysis of samples showed that on increasing Sn-Zn content the grain size decreased. It was also observed that by increasing the substitution content in the ferrite thin films, the coercivity value and saturation magnetization values increased but magnetic interaction reduced.

XiansongLiuet. al. [23] synthesized strontium hexa-ferrite by ceramic process where Sr⁺² was substituted by La⁺³ and Fe⁺³ was substituted by Co⁺² according to the formula $\text{Sr}_{1-x}\text{La}_x\text{Fe}_{12-x}\text{Co}_x\text{O}_{19}$. It was observed that when an appropriate amount of substitution of

La³⁺ and Co²⁺ was done then an increase in saturation magnetisation and intrinsic coercivity resulted.

Ali Ghasemi [24] prepared SrFe_{12-x}(Zr_{0.5}Mg_{0.5})_xO₁₉ by sol-gel method where x = 0 to 2.5. The magnetic properties of this sample was studied with the help of a vibrating sample magnetometer (VSM) and it was observed that with an increase in Zr-Mg substitution content the coercivity decreases but saturation magnetisation value increases.

Kubo et. al. [25] invented a composite type magnetic particles (A) each of which contains hexagonal ferrite and spinel structure ferrite and single phase type magnetic particles of hexagonal ferrite (B). This type of magnetic particle has a stronger resistance to noise than that made by using single phase type magnetic particles of hexagonal ferrite thereby providing excellent electromagnetic characteristics. This also provides a higher signal to noise ratio for short wavelength range. The formula for the compound is AOn(Fe_{12-x-y}M(1)_xM(2)_yO_{18-z}) where A = Ba / Sr / Ca / Pb , M(1) = Co / Zn / Ni / Cu / Mn / Fe, M(2) = Ti / Sn / Ge / Zr / Sb / Nb / V / Ta / W / Mo. X can vary from 0.5 to 0.3 , Y from 0 to 2.0 and Z can be 0.05 or larger. When A: B=5:95 or 30:70 it can be used as a magnetic recording medium for 1μm wavelength or lower and when A: B = 70: 30 to 95: 5 it can be used for 1μm wavelength or higher.

Wandee Onreabroyet. al. [20] investigated the structural and magnetic properties of Sr_{0.8}La_{0.2}Fe₁₂O₁₉ which were fabricated by conventional ceramic process. It was observed by studying the XRD patterns that the undoped sample had a hematite phase which was much lower in case of the doped specimen. By SEM analysis it was also observed that by the doping of La³⁺ caused a lesser increase in average grain size as compared to the undoped

specimen. The study also showed that the doped sample had higher values of saturation magnetization than before.

Objective of this project

Objective of the present work is to investigate the effect of CuO addition on the (a) phase formation, (b) phase stability, (c) Dielectric and (d) Magnetic properties of Zn-Ti substituted Sr-M Hexagonal ferrite.

Chapter 3

Experimental procedure

The strontium M-ferrite with **composition: $\text{SrZn}_{1.3}\text{Ti}_{1.3}\text{Cu}_x\text{Fe}_{9.4-x}\text{O}_{19-z}$** has been prepared through sol-gel auto combustion route. Following chemical precursors were used for the synthesis of the ferrite:

1. Strontium nitrate [$\text{Sr}(\text{NO}_3)_2$]
2. Iron nitrate [$\text{Fe}(\text{NO}_3)_3$]
3. Zinc nitrate [$\text{Zn}(\text{NO}_3)_2 \cdot 6\text{H}_2\text{O}$]
4. Titanium oxide [TiO_2]
5. Copper nitrate [$\text{Cu}(\text{NO}_3)_2 \cdot 3\text{H}_2\text{O}$]

All the chemical used were of analytical grade with 99.8% purity. Citric Acid [$\text{C}_6\text{H}_8\text{O}_7 \cdot \text{H}_2\text{O}$] was used as fuel in the auto combustion method. Tetra-isopropyl-ortho-titanate ($\text{C}_{12}\text{H}_{28}\text{O}_4\text{Ti}$) was used as source of TiO_2 in the synthesis.

Sol-gel combustion synthesis:

Pure and Zn-Ti substituted $\text{SrFe}_{12}\text{O}_{19}$ (SrM) ferrite powders were synthesized by sol-gel auto combustion process. This process has advantages such as low energy consumption, simple equipment requirement, simple preparation method and soluble precursors which give homogeneous, nano-sized, highly reactive powders [26]. The auto combustion synthesis process also known as self-propagating synthesis was first developed by Merzhanov and had been used successfully in preparation of complex oxides like ferrites [27].

Sol-gel auto-combustion synthesis route involves exothermic redox reaction between organic fuel and a metal nitrate to yield multi-element oxide. The auto-combustion synthesis is self-sufficient to provide the energy required for the reaction to take place. The organic fuel along with metal nitrates is mixed in distilled water to form a solution which maximizes the molecular mixing of the constituent components. This solution is then slowly heated to dry and ultimately transform it to a gel. The gel eventually ignites in a self-propagating combustion manner until all the gel is completely burnt out. This self-propagating combustion reaction lasts about 5-10 seconds to yield the desired product. This route yields a highly homogeneous product in a very short period of time. The parameters that influence an auto-combustion synthesis reaction are fuel to oxidizer ratio (f/o), ignition temperature, water content of the precursor mixture and the type of fuel used. The fuel to oxidizer ratio is critical

from the reaction point of view. The flame temperature of the reaction can be controlled by varying ratio of fuel to oxidizer.

Ferrite powder was synthesized by an amount of 15 gm. per batch. Briefly to prepare 15 gm. $\text{SrZn}_{1.3}\text{Ti}_{1.3}\text{Fe}_{9.4}\text{O}_{19}$ ferrite, 2.984 gm strontium nitrate, 5.453 gm. Zinc nitrate, 1.465 gm. titanium oxide, 53.546 gm. Iron nitrate and 88.851 gram of citric acid was mixed in to the solution. The flow-chart of the synthesis is shown in Fig.3.

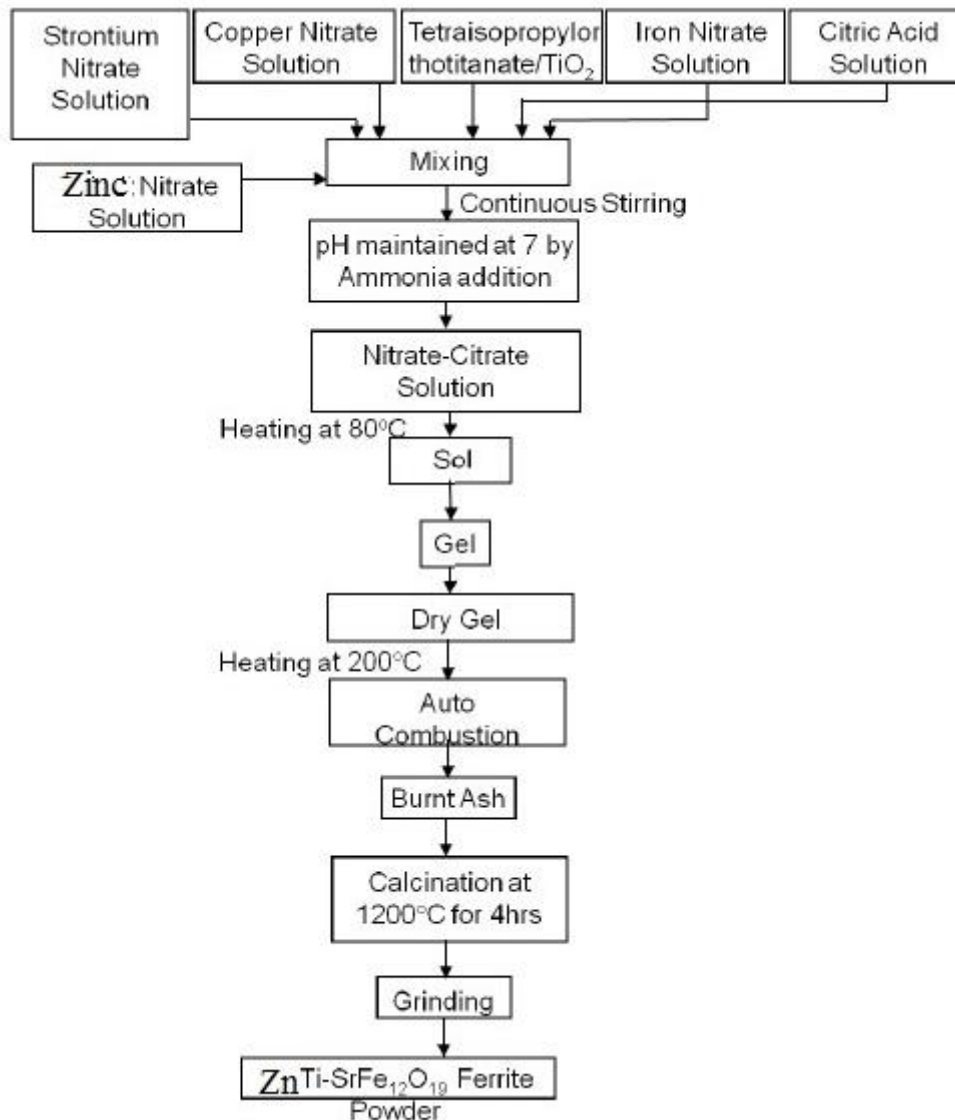


Fig-3: Flow diagram for auto combustion synthesis of $\text{SrFe}_{12}\text{O}_{19}$ ferrite powder

In Zn, Ti, CuO substituted $\text{SrFe}_{12}\text{O}_{19}$; required moles of constituents were added to the solution before the addition of citric acid. The mixture thus obtained was placed in a beaker and was homogenized by stirring. The pH of the solution was approximated to 7 by the addition of ammonia solution. Then the solution was heated slowly on a hot plate at a

temperature of 80°C. This continuous slow heating gives rise to a sol which then converts to a gel. The gel thus obtained was dried at 200°C until the gel ignited in a self-propagating combustion manner and finally yielding a fluffy structured material. This fluffy material was further ground and again calcined at 1200°C for 4 hours. Calcined powder was ground to get ferrite powder.

Dried gel and powder characterization:

Thermal Characterization:

The dried gel was characterized by differential scanning calorimetry (DSC) and thermo gravimetric analysis (TGA) using NETZSCH STA (Model No 409C). This technique is excellent to get an idea about decomposition behaviour, phase transitions, formation of products, etc. of precursor powders synthesized through different routes. TGA is a simple analytical technique that measures the weight loss (or weight gain) of a material as a function of temperature. As materials are heated, they can lose weight due to drying, or from chemical reactions that liberate gasses. Some materials can gain weight by reacting with the atmosphere in the testing environment. In DSC, heat flux required to maintain the temperature of both test sample and inert sample is measured. This heat flux is measured in mW/mg.

Dried gel and powder characterization

Phase Analysis

The phase formation characteristic of the burnt and calcined powder was studied by using powder X-ray Diffraction performed with the help of Rigaku's Diffractometer (model- Ultima 4, Japan). For the detection of diffracted X-rays, there is an electronic detector on the other side of the sample in the X-ray tube. The sample is rotated through different Bragg's angles. The track of the angle (θ) is kept with the help of a goniometer, the detector records the detected X-rays in counts/sec and sends this data to the computer. After the complete scan of the sample the X-ray intensity versus angle theta (2θ) is plotted. The angle (2θ) for each diffraction peak is then converted to d -spacing, using the Bragg's law; $n\lambda = 2d \sin\theta$, where λ is the wave length of x-ray and n is order of diffraction. The phases that were present in the sample were identified by the help of Philips X-pert high score software.

Fabrication and sintering of ferrite parts

The powder of each batch which was earlier calcined at 1200°C for 4 hours was mixed with 5 wt% binder (polyvinyl alcohol). The following flow diagram (Fig.4) shows the entire process. Initially the calcined powders were mixed with 5 wt% PVA binder solution for about 2 hours and then dried at about 50°C. Then the resulting specimen was granulated and then pressed in the form of pellets with diameter-13mm, and thickness- < 3mm using a uniaxial hydraulic press at a pressure of 4 Tonnes for 90 seconds.

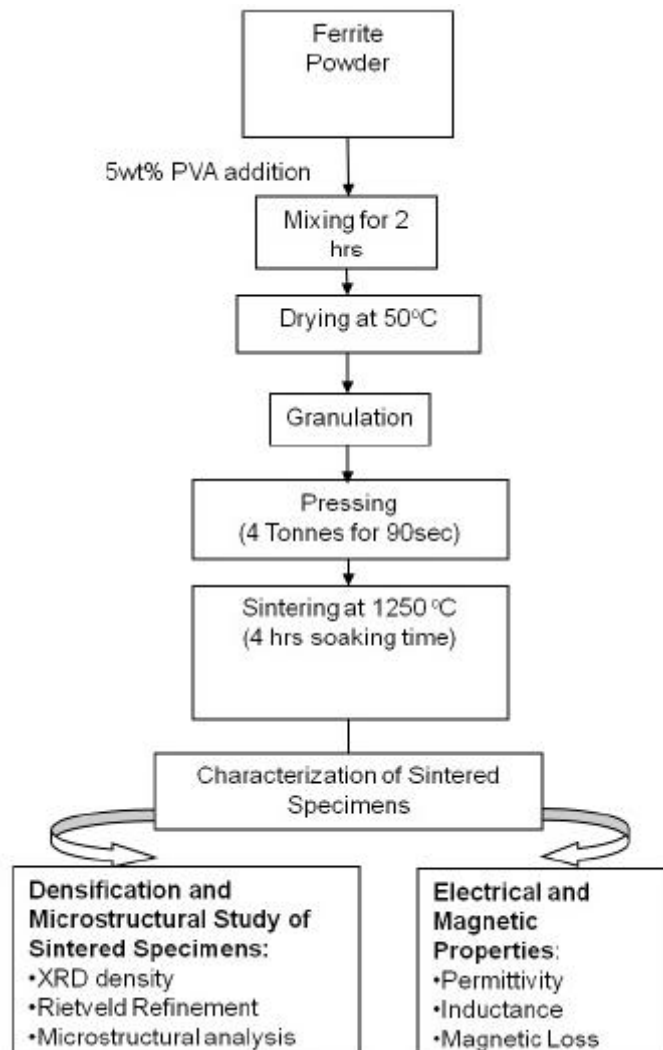


Fig-4: A flow chart of fabrication and characterization for sintered ferrite parts.

The pressed pellet samples were sintered in an electric furnace at various temperatures. The thermal regime of the furnace was controlled through a “Eurotherm” programmer-cum-controller within $\pm 2^\circ\text{C}$ accuracy. The pellet samples were heated from room temperature to 650°C at 1°C/min followed by soaking at 650°C for 2 hours and then heating at 3°C/min till

the sintering temperature and then soaking at the sintering temperature for 4 hours. Then the samples were cooled inside the furnace till room temperature was reached.

Characterization of Sintered Specimens

Density and Apparent Porosity

Bulk density and apparent porosity of sinter specimens were determined by Archimedes principle. Sintered samples were weighted in dry state. Samples were immersed in water and kept under a vacuum of 4 mm of mercury for 5 hrs to ensure that water filled up the open pores completely. Then, soaked and suspended weights were measured. The apparent porosity and bulk density were calculated as follows:

Dry weight of the sample = W_d , Soaked weight of the sample = W_s , Suspended weight of the sample = W_a

$$\% P_{\text{App}} = \frac{W_s - W_d}{W_s - W_a} \times 100$$

$$D_{\text{bulk}} = \frac{W_d}{W_s - W_a}$$

Microstructural Analysis

The microstructures of the sintered pellets were studied with the help of Field Emission Scanning Electron Microscopy (FESEM). The FESEM has an electron gun which under vacuum conditions emits a beam of electrons which is allowed to pass through a series of electromagnetic lenses before falling on the surface of the sample. The voltage range of the electron beam is in the range of 1-30 kV. When the electron beam interacts with the surface of the sample a part of it is reflected as back scattered electron (BSE) and also as low energy secondary electron (SE), cathode luminescence, X-ray excitation beam and some part of the electron beam is transmitted.

The secondary electron beam forms an image which is studied in the extrinsic mode of SEM. These secondary electrons are then displayed on a television screen. The image thus formed would be bright if there is high secondary electron emission and this type of high emission is due to surface structure of the sample. The final picture which is obtained has brightness associated with surface characteristics and the image is normally illuminated. The samples

were mounted on a metal stub with carbon paint. The mounted samples were studied by SEM (FEI).

Dielectric characterization

For the dielectric characterization the sintered pellet samples were first cleaned with acetone and then a layer of silver paste was applied on the top and bottom surface of each pellet. Then these pellets were cured in a furnace at 650°C for 30 mins. After curing the dielectric test of these samples was carried out.

The device used for this characterization was LCR HiTESTER (Model 3532-50) HIOKI. The measurements for this test were taken in the range of 100Hz to 1MHz. The graphs of $\tan \delta$ vs frequency and permittivity vs frequency were plotted and analysed, where $\tan \delta$ = dissipation or loss factor and relative permittivity is:

$$\epsilon' = \frac{C \times d}{\epsilon'' \times A}$$

ϵ'' = relative permittivity of air (8.854×10^{-12} F m⁻¹)

C = capacitance

d = thickness of pellet

A = area of the top surface of pellet.

Inductance and Magnetic Loss

Magnetic loss and inductance are the most primary magnetic characteristic property of any ferrite. The instrument that was used to measure this property was the LCR HiTESTER (Model 3532-50) HIOKI. This instrument was used to measure $\tan \delta$ and inductance on toroid samples which were wound by low capacitive six turns of enamelled copper wire. The importance of this winding is that the stray capacitance (unwanted capacitance which can allow signals to leak between circuit wires) can be reduced by this special winding of the ferrite core.

The inductance of a ferrite core depends upon length of the coil, number of turns, diameter of the coils and the nature of the ferrite composition. Inductance is the ratio of the total magnetic flux linkage to the current (I) through the ferrite core. The total magnetic flux linkage depends on magnetic permeability (μ) of the medium or core material. This tells us that magnetic inductance is directly proportional to magnetic permeability. The initial permeability was calculated from the data of inductance by the use of the following formula:

$$\mu' = \frac{L}{2 \times 10^{-7} \times N a^2 \times H_t \times \ln \left[\frac{D_o}{D_{in}} \right]}$$

Where L = inductance

Na = number of turns

Ht = height of toroid

Do = outer diameter of the toroid

Din = inner diameter of the toroid

Many core losses which occur in cases of ferrites are due to hysteresis loss, eddy current losses and residual losses. The generation of hysteresis loss is due to irreversible rotation of magnetization vector. The eddy current loss is generated due to the current induced in the core under the influence of a time varying magnetic flux. The residual loss is caused by the power dissipation due to the reversible domain wall damping and the reversible rotation of domains. The relative loss factor (RLF) which is the ratio of $\tan \delta$ (loss tangent) to μ' (initial permeability) was calculated.

Chapter-4

Results and discussion

Results and Discussion

The thermal decomposition behaviour of gel was studied by differential scanning calorimetric (DSC) and thermo gravimetric (TG) analysis. **Fig. 5** shows the DSC-TG plot. The DSC plot shows 2 exothermic peak at 343°C and 392°C. The small DSC peak at 343°C is due to removal of residual organic fuel. The combustion process, an exothermic one, can be considered as a thermally induced anionic redox reaction of the gel in which the carboxyl groups act as reductant and NO_3^- ions act as oxidant.

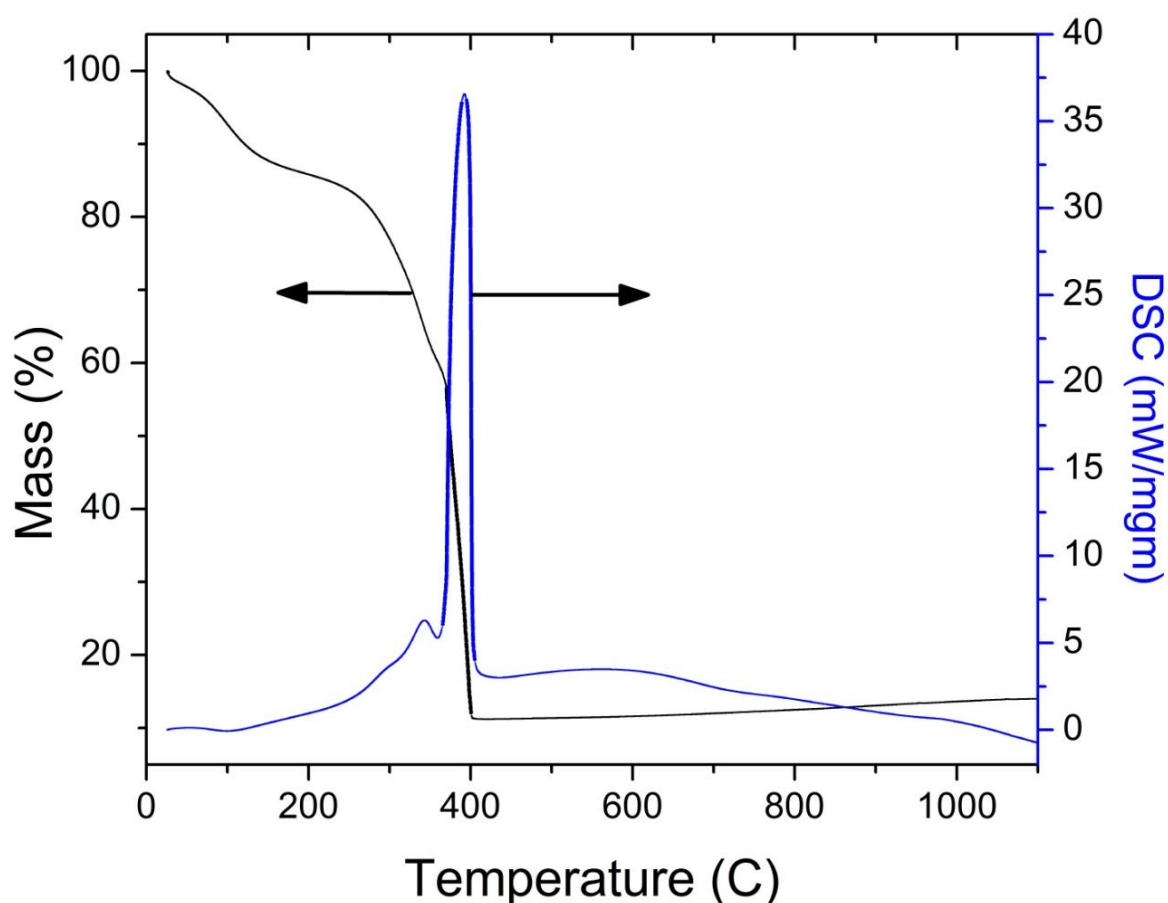


Fig 5 DSC-TG plots for the nitrate-citrate gel with a heating rate of 10°C /min in air atmosphere.

In the combustion process, heat is released which supply the energy needed to react the components to form Sr-Zn-Ti-ferrite through solid-state diffusion process. During combustion CO_2 , N_2 , and H_2O gasses are released. The TGA curve exhibited two step weight losses, one in the range of 75-200°C and other in range of 300-400°C. The autocatalytic combustion process occurred at 390°C causing 71.9% weight loss.

Phase Evolution

Fig. 6 shows the XRD pattern of calcined powder for 3 compositions. Without CuO containing specimen was calcined at 1100 degree Celsius. The figure 6a shows the XRD pattern of the calcined powder. It shows that 45% phase formation and 55% un-reacted iron oxide present in the powder. For that reason, calcination temp was increased to 1200. Fig 6b and 6c shows the XRD pattern of 0.5% and 1.0% CuO containing specimen those calcined at 1200.

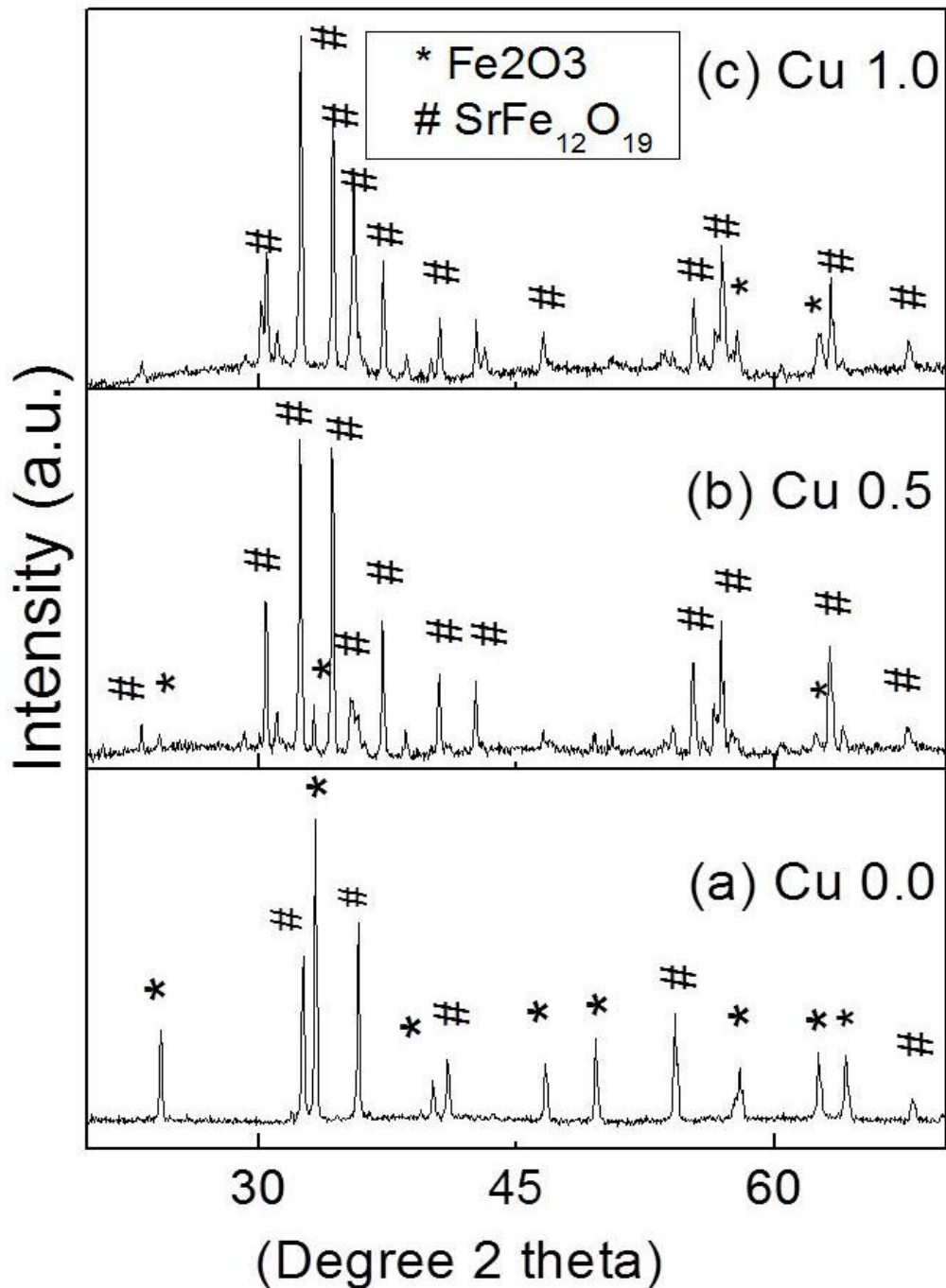


Fig 6: XRD pattern of calcined ferrite powder.

0.5% Cu doped powder XRD pattern shows that the desired SrM ferrite phase formation was almost completed. The semi quantitative estimation showed that SrFe₁₂O₁₉ (pdf no-79-1412) was about 90% and unreacted iron oxide (pdf no-73-2234) is about 10%.

However 1.0% copper added specimen powder showed that there is almost 100% ferrite phase formation and no unreacted iron oxide peaks were found. So it indicates that increasing copper addition helps in phase formation behaviour of ferrite. This may be due to the formation of liquid phase assisted by CuO which helps in easy reaction through liquid phase diffusion mechanism.

Fig. 7 shows the XRD pattern of sintered ferrites. 0.0 wt% CuO specimen (Fig. 7 (a)) shows almost 90% pure ferrite phase and 10% un-reacted iron oxide in the composition. So it clearly indicates that the sintered pellets shows better phase than only calcined ferrite powders.

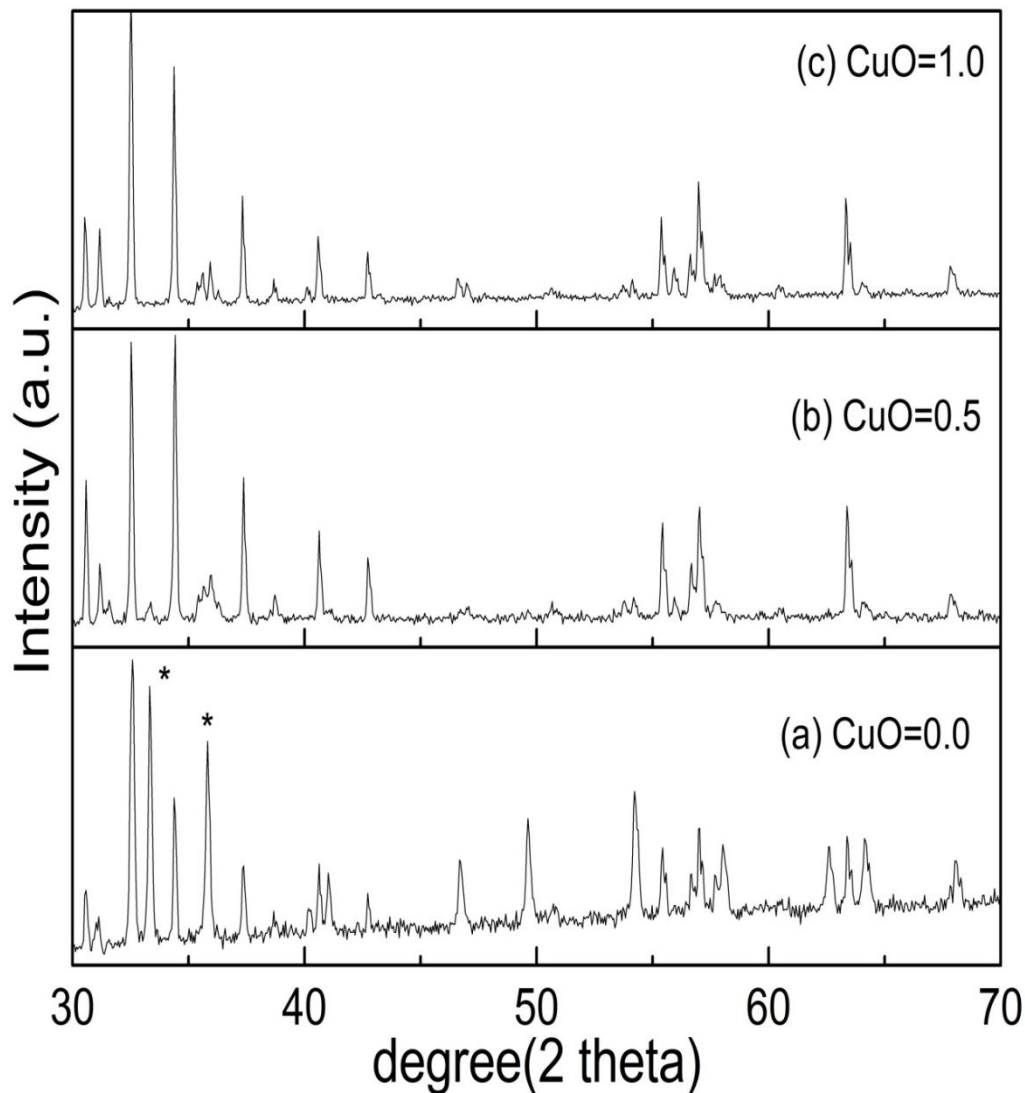


Fig 7: XRD pattern of sintered pellets fired at 1250 °C.

0.5 wt% CuO specimen (Fig 7b) shows almost pure ferrite phase however there was about 5% un-reacted iron oxide.

Fig 7c shows the XRD pattern of 1wt% CuO containing sintered pellet specimen. It shows a pure ferrite phase. This result also indicates that CuO addition helps in phase formation behaviour of SrM ferrite.

Bulk Density and Apparent Porosity

Fig. 8 shows the behaviour of bulk density and apparent porosity of ferrites. With increase in amount of CuO, bulk density normally increases and apparent porosity decreases as shown in the figure. This may be due to the effect of CuO assisted liquid phase sintering. This indicates that CuO is helping in sintering in a limited way.

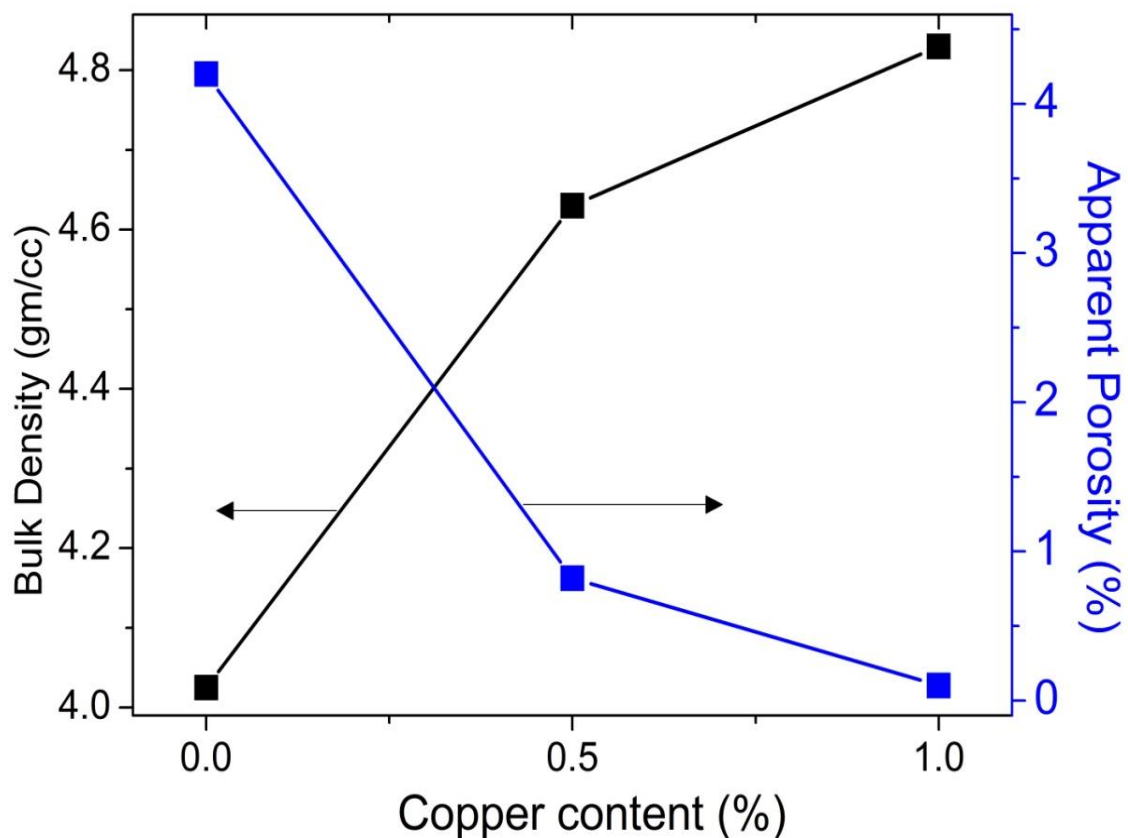


Fig 8 Bulk density and apparent porosity of sintered pellets.

Dielectric property

Fig.9 shows that permittivity of specimen decreases with increase in frequency which is the typical phenomenon. Also it indicates that permittivity decreases with increase in copper content and it is lowest in 1% CuO composition. So the 1% CuO composition will be the best material among all for inductor core application. Moreover its permittivity is very stable with the change in frequency in the MHz range. This CuO-doped material is suitable for a stable high frequency application.

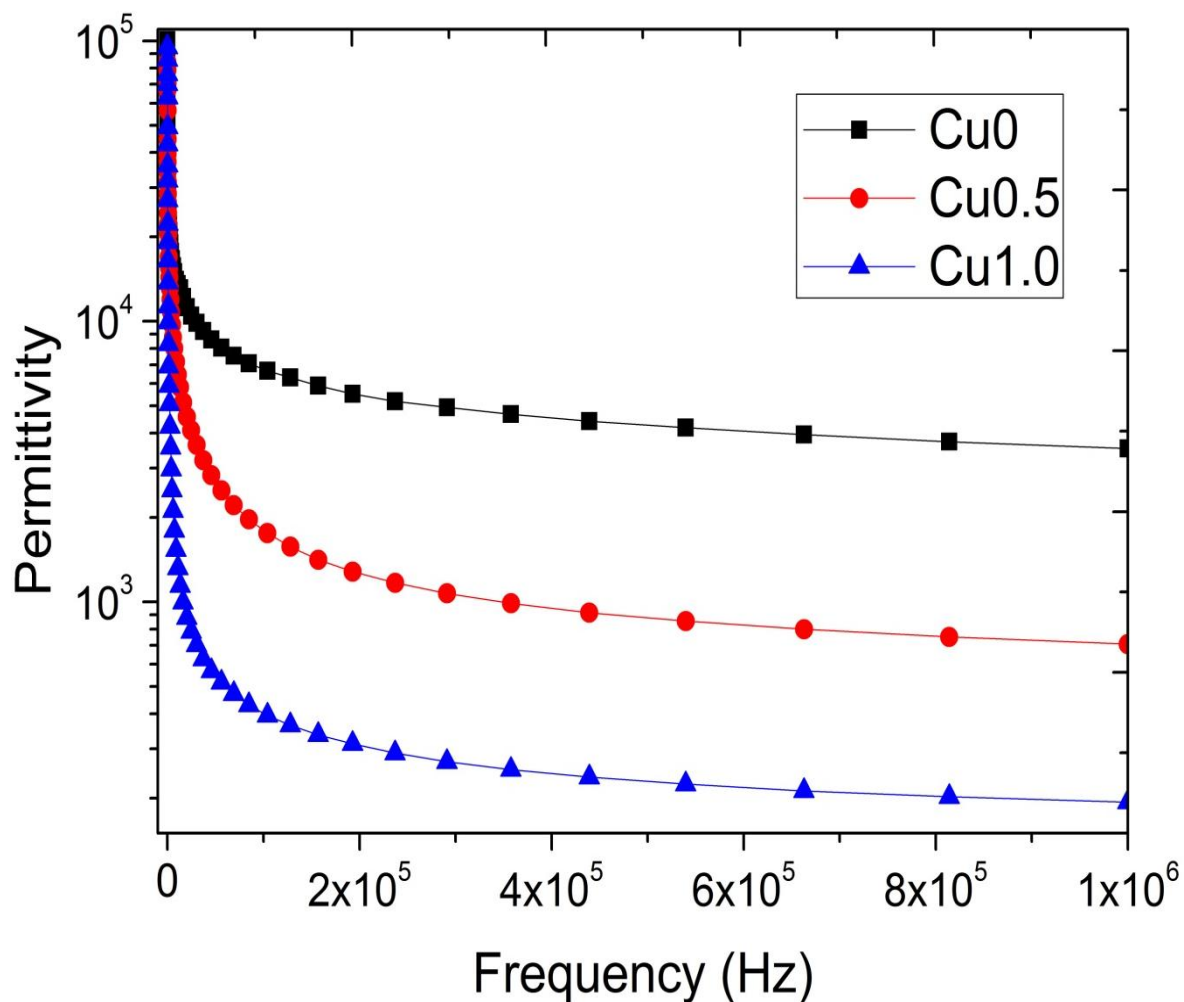


Fig 9 Frequency dependency of initial permeability in ferrites with different CuO content.

Fig. 10 shows the variation of dielectric loss (tan delta) with frequency. It shows that dielectric loss decreases with increase in frequency at higher frequency. Also addition of CuO results in increase of dielectric loss because resistivity of the samples decreased with increase in CuO content. The loss factor is a very important parameter for Multi-Layer Chip Inductor (MLCI).

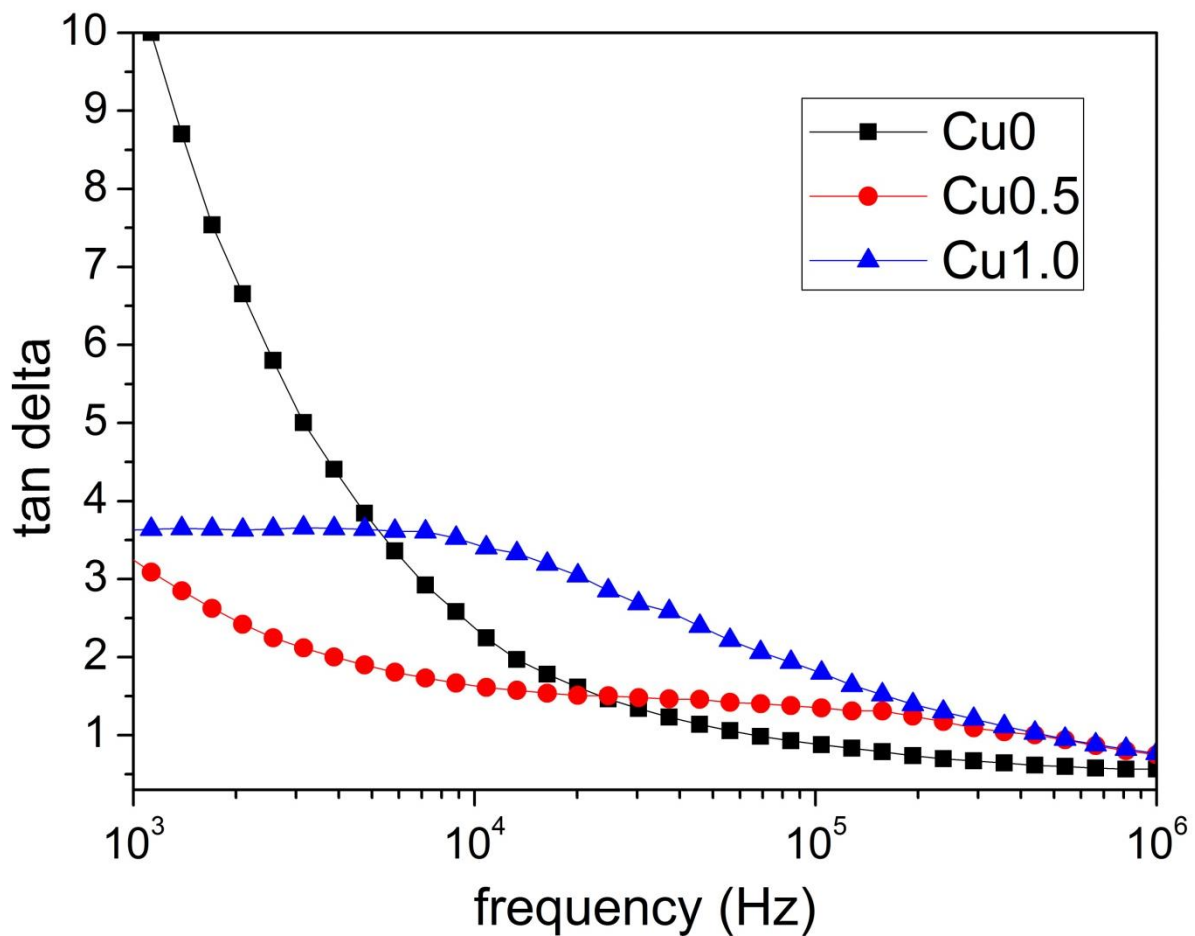


Fig 10: Frequency dependency of dielectric loss factor in different CuO content ferrites.

Magnetic property:

Fig. 11 shows the variation of initial permeability with frequency. Initial permeability decreases with increase in frequency because the switching of magnetic domains is restricted by domain walls and so their response decreases significantly at higher frequencies. With

increase in CuO content, initial permeability increases. This is due to the higher density and higher grain size of the ferrite created by CuO addition.

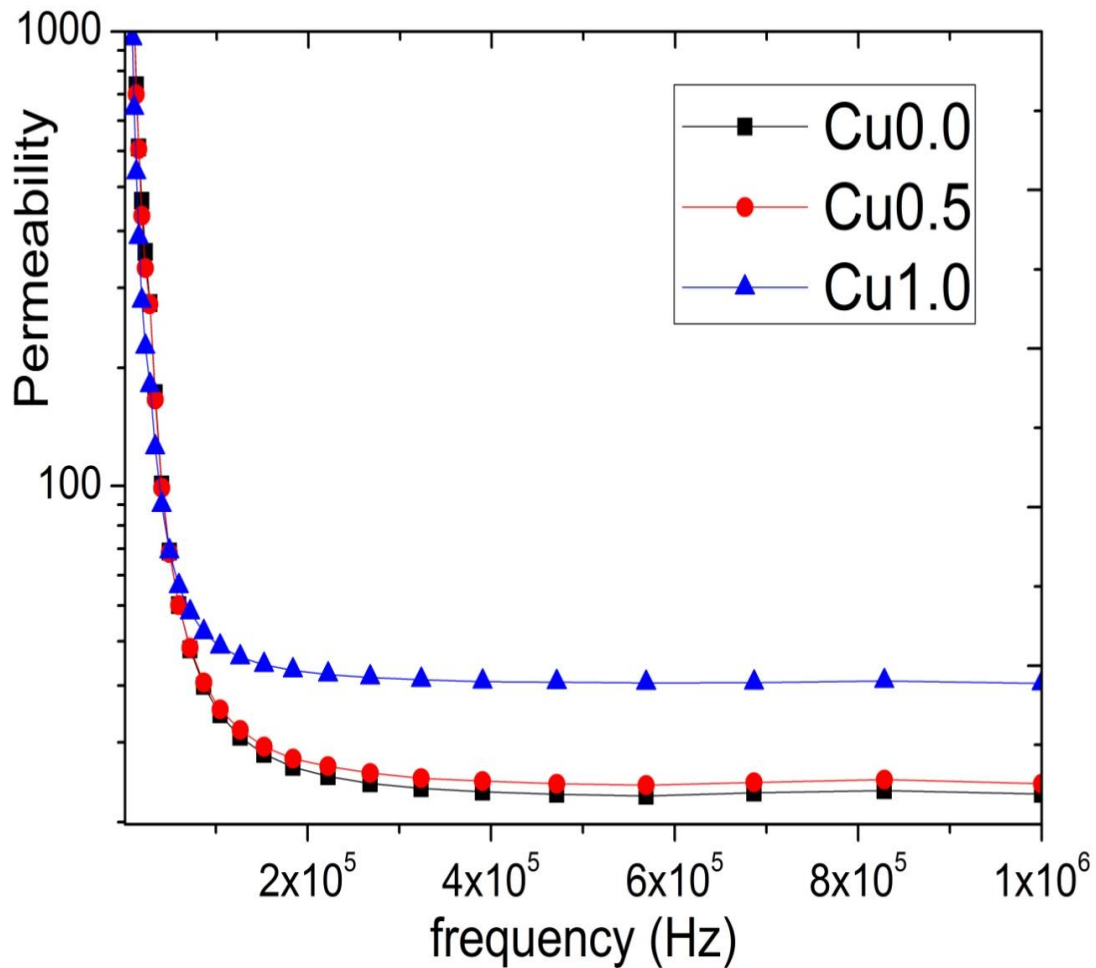


Fig 11 Dependence of initial permeability on frequency for different ferrite compositions.

Fig. 12 shows the variation of relative loss factor with frequency for different ferrite composition. The ratio of magnetic loss to initial permeability (μ') is known as Relative Loss Factor (RLF). RLF is an important parameter for the inductors to be used at higher frequency and a low RLF is desirable. RLF decreases with increasing frequency and also with

increasing amount of CuO in the composition. The composition having Cu-1.0 weight % has lowest RLF due to its highest permeability.

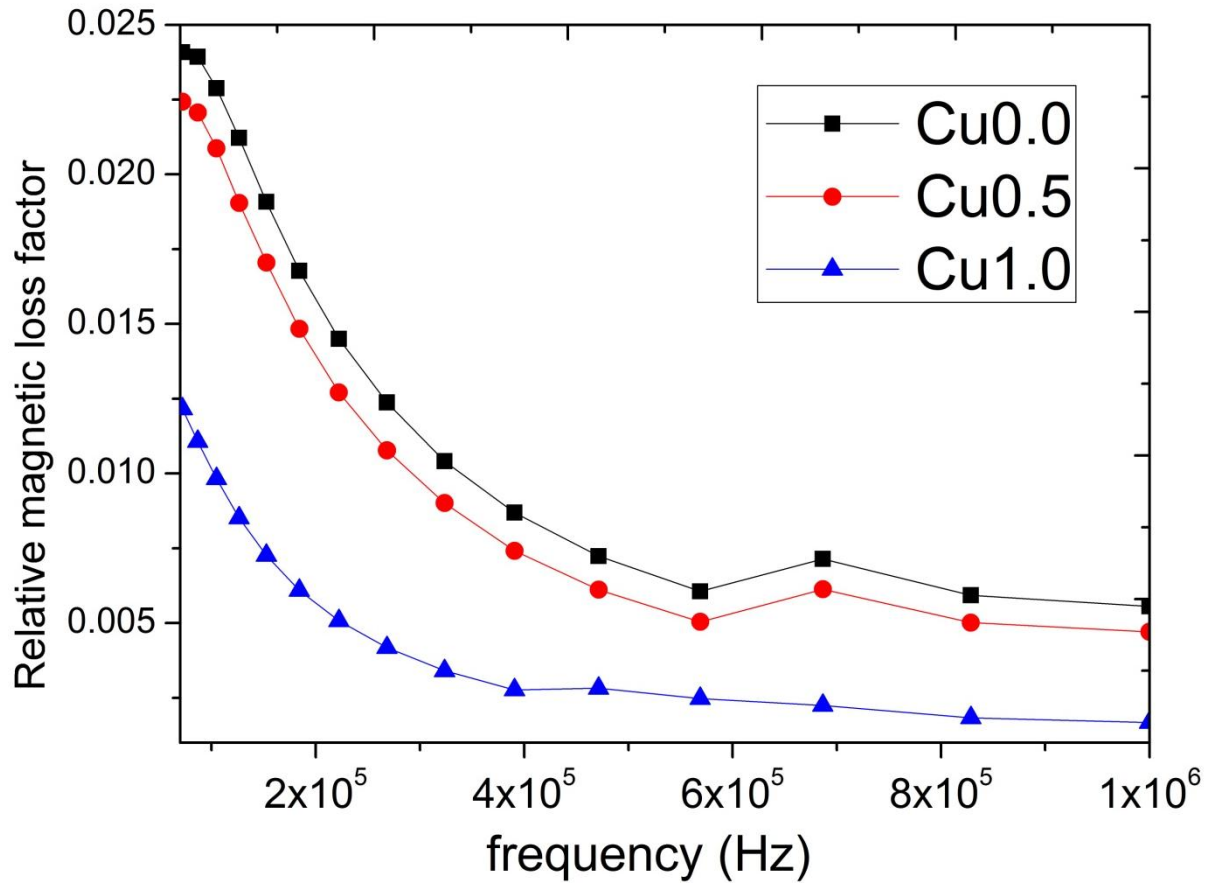


Fig 12: Variation of relative loss factor for torroids of different compositions with frequency.

Microstructural analysis

Fig. 13 shows the SEM microstructure of three compositions. Fig shows that upon CuO addition grain size increases. Also there is change in grain shapes which is prominent in the samples containing CuO-0.5 and CuO-1.0. The highest grain size was observed in in CuO-1.0 specimen with an average grain size of around 6 μ m. Also CuO-1.0 specimen is very compact.

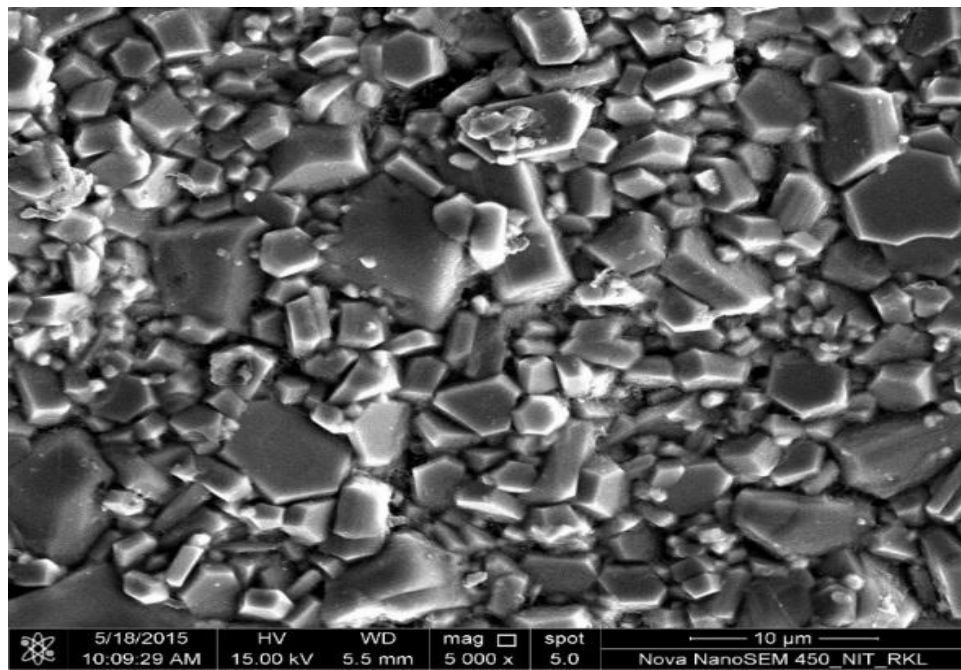
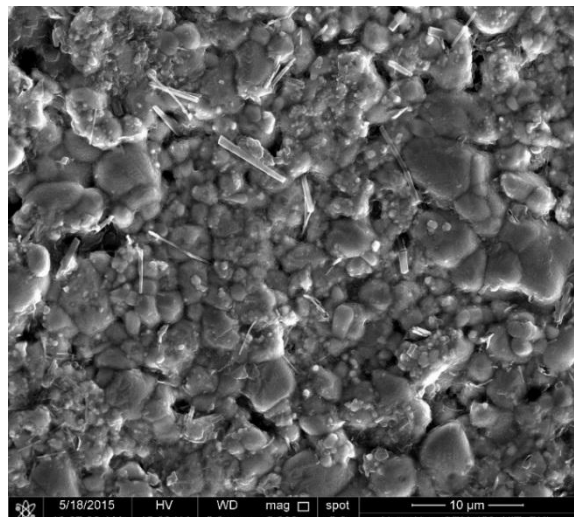
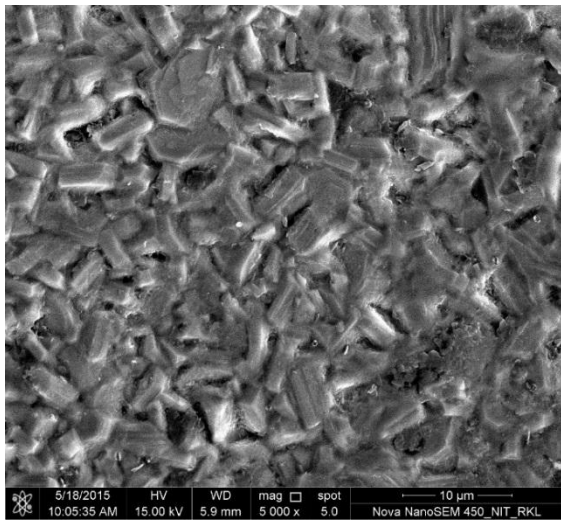


Fig 13: SEM images of sintered pellets.

Chapter 5

CONCLUSION

Conclusion:

Effect of CuO addition on the properties of Zn & Ti substituted Sr-M hexagonal ferrite has been investigated. $\text{SrZn}_{1.3}\text{Ti}_{1.3}\text{Cu}_x\text{Fe}_{9.4-x}\text{O}_{19-z}$ ferrite has been synthesized successfully through citrate gel combustion process. Pure phase ferrite was produced after calcination of as burned powder at 1200°C . CuO was added in the ferrite in an amount $x=0.5$ & 1.0 in the formula stated above. Undoped ferrite composition showed presence of un-reacted Iron Oxide. It was found that the ferrite phase formation was maximum at a value of CuO $x=1.0$. This may be due to the effect of CuO addition which forms liquid phase & accelerate the formation of the ferrite phase. Bulk density of ferrite was found to increase rapidly with the addition of CuO. Similarly, apparent porosity also decreased. The dielectric permittivity of CuO added Ferrite was lowest. However, the dielectric loss was higher in copper oxide added specimen in MHz frequency range. The magnetic permeability of copper oxide added Ferrite was higher than the un-doped ferrite due to the better densification of CuO added ferrite. Also, copper oxide added ferrite has bigger grain size. Relative magnetic loss factor was lowest in copper oxide added ferrite. So, it may be concluded that, CuO is an effective sintering additive for Sr-M- Hexagonal Ferrite.

Chapter-6

References

REFERENCES

- [1] Smit J, Wijn HPJ. Ferrites, Philips Technical Library, Eindhoven; 1959.
- [2] Robert C. Pullar, Progress in Materials Science 57 (2012) 1191–1334
- [3] J. Mürbe, J. Töpfer, Journal of the European Ceramic Society 32 (2012) 1091–1098
- [4] Nobuyoshi Koga, Takanori Tsutaoka, Journal of Mag and Mag Mate. 313 (2007) 168–175
- [5] United States Patent Application Pub. No.: US 2012/0085963 A1, Apr.12, 2012.
- [6] http://www.tdk.co.jp/techjournal_e/vol04_mlg/contents04.htm
- [7] Silvia Bierlich, Jörg Töpfer, IEEE Transactions On Magnetics, Vol. 48, No. 4, 2012
- [8] T. Tachibana, T. Nakagawa, Y. Takada, T. Shimada, and T. Yamamoto, J. Magn. Mater. vol. 284, pp. 369–375, 2004.
- [9] Y. Bai, J. Zhou, Z. Gui, and L. Li, J. Magn. Mater., vol. 246, pp. 140–144, 2002.
- [10] S. Bierlich, J. Töpfer, J. Magn. Mater, 324 (2012) 1804–1808
- [11] S. Kraunovská and J. Töpfer, J. Magn. Mater, vol. 320, pp. 1370–1376, 2008.
- [12] Narang SB, Huidara LS. J Ceram Process Res 2006;7:113.
- [13] Yamamoto H, Kumehara H, Takeuchi R, Nishio N. J Phys IV 1997;7:C1–535.
- [14] Pullar RC, Taylor MD, Bhattacharya AK. J Mater Res 2001;16:3162.
- [15] Jean M, Nachbaur V, Bran J, Le Breton J-M. J Alloys Compd 2010; 496:306.
- [16] Sato H, Umeda T. In: Ferrites, proc ICF6, Kyoto and Tokyo; 1992. p.1122.
- [17] Zhong W, Ding W, Jiang Y, Zhang N, Zhang J, Du Y, et al. J Am Ceram Soc 1997;80:3258.
- [18] R. Lebourgeois, “Ferrite Material for a Permanent Magnet and Method for Production”; Patent: WO 2004/102595, PCT/EP2004/050825, May 17th 2004.

- [19] M.N. Ashiq, R.B. Qureshi, M.A. Malana, M.F. Ehsan, Synthesis, Structural, Magnetic and Dielectric Properties of Zirconium Copper doped M-type Calcium Strontium Hexaferrites, *Journal of Alloys and Compounds* (2014).
- [20] Wandee Onreabroy, Komane Papato, Gobwute Rujjanagul, Kamonpan Pengpat, Tawee Tunkasiri. *Ceramics International* 38S (2012) S415–S419.
- [21] Ali Ghasemi, Vladimir ˇSepela´k, *Journal of Magnetism and Magnetic Materials* 323 (2011) 1727–1733
- [22] Qingqing Fang, Yanmei Liu, Ping Yin, Xiaoguang Li. *Journal of Magnetism and Magnetic Materials* 234 (2001) 366–370
- [23] Xiansong Liu, Pablo Herna´ndez-Go´mez, Kai Huang, Shengqiang Zhou, Yong Wang, Xia Cai, Hongjun Sun, Bao Ma. *Journal of Magnetism and Magnetic Materials* 305 (2006) 524–528
- [24] Ali Ghasemi. *Journal of Magnetism and Magnetic Materials* 324 (2012) 1375–1380
- [25] Kubo et. al. US patent No. 5378547
- [26] Z. Yue, L. Li, J. Zhou, H. Zhang, Z. Gui, *Mat. Sci. Engg. B* 64 (1999) 68.
- [27] M. D. Nersesyan, A. G. Peresada, A.G. Merzhanov, *Int. J. SHS* 7 (1998) 60.